Diamond & Related Materials 136 (2023) 109939

Contents lists available at ScienceDirect

Diamond & Related Materials

journal homepage: www.elsevier.com/locate/diamond

Soliton compression and supercontinuum spectra in nonlinear diamond photonics

O. Melchert [a,b,*], S. Kinnewig [b,c], F. Dencker [d], D. Perevoznik [a], S. Willms [a,b], I. Babushkin [a,b], M. Wurz [d], M. Kues [b,e], S. Beuchler [b,c], T. Wick [b,c], U. Morgner [a,b], A. Demircan [a,b]

[a] Leibniz Universität Hannover, Institute of Quantum Optics, Welfengarten 1, Hannover 30167, Germany
[b] Leibniz Universität Hannover, Cluster of Excellence PhoenixD, Welfengarten 1A, Hannover 30167, Germany
[c] Leibniz Universität Hannover, Institute of Applied Mathematics, Welfengarten 1, Hannover 30167, Germany
[d] Leibniz Universität Hannover, Institute of Micro Production Technology, An der Universität 2, Garbsen 30823, Germany
[e] Leibniz Universität Hannover, Institute of Photonics, Nienburger Str. 17, Hannover 30167, Germany

ARTICLE INFO

Keywords:
Diamond
Generalized nonlinear Schrödinger equation
Supercontinuum generation
Pulse self-compression

ABSTRACT

We numerically explore synthetic crystal diamond for realizing novel light sources in ranges which are up to now difficult to achieve with other materials, such as sub-10-fs pulse durations and challenging spectral ranges. We assess the performance of on-chip diamond waveguides for controlling light generation by means of nonlinear soliton dynamics. The considered silica-embedded diamond waveguide model exhibits two zero-dispersion points, delimiting an anomalous dispersion range that exceeds an octave. Various propagation dynamics, including supercontinuum generation by soliton fission, can be realized in diamond photonics. In contrast to usual silica-based optical fibers, where such processes occur on the scale of meters, in diamond millimeter-scale propagation distances are sufficient. Unperturbed soliton-dynamics prior to soliton fission allow identifying a pulse self-compression scenario that promises record-breaking compression factors on chip-size propagation lengths.

1. Introduction

Nonlinear diamond photonics provides an attractive technical basis for on-chip photonic applications [1], and has triggered numerous research efforts in recent years. Owing to the unique material properties of diamond [2,3], given by its large Kerr nonlinearity, wide bandgap, high refractive index, negligible multi-photon loss, and transmission window spanning from the ultraviolet to the far-infrared, impressive demonstrations of photonic devices with novel functionalities have emerged. This includes, e.g., its use as a platform for quantum communication [4], and integrated high-Q optical resonators [1,5], operating at new wavelengths compared to existing chip-based nonlinear photonic devices for frequency comb generation [3,6]. It thus exceeds its use in quantum optics applications and is becoming a versatile material for optical devices. A direct transfer of concepts from photonic crystal fibers and silicon-based waveguides [7,8], such as, e.g., pulse-compression schemes and soliton-effects, to the diamond-based platform seems possible.

Here, we consider the supercontinuum generation process [9–12], a paradigm of optical pulse propagation in fibers, which has revolutionized optical coherence tomography [13], and frequency metrology [14]. In common silica-based photonic crystal fibers, this process occurs on the lengthscale of several centimeters [15], or even meters [9]. We use the propagation properties of a diamond waveguide surrounded by silica [1], and demonstrate in terms of numerical simulations that the supercontinuum generation process unfolds on a much shorter, millimeter-length propagation scale. In our analysis, we investigate the propagation dynamics of ultrashort optical pulses via the generalized nonlinear Schrödinger equation [10], taking into account higher-order dispersion, pulse self-steepening [16,17], and the Raman effect [18]. This accounts for various processes that support the generation of widely extended supercontinuum spectra, such as the modulation instability [19], soliton-fission [20,21], and self-frequency shift of Raman solitons [18]. The initial stage of the supercontinuum generation process allows identifying a pulse self-compression mechanism based solely on soliton-effects [22]. The dependence of the maximum degree of compression, achieved by this soliton compression method, and the corresponding optimal propagation length on the initial pulse parameters have been

* Corresponding author at: Leibniz Universität Hannover, Institute of Quantum Optics, Welfengarten 1, Hannover 30167, Germany.
E-mail address: melchert@iqo.uni-hannover.de (O. Melchert).

https://doi.org/10.1016/j.diamond.2023.109939
Received 1 November 2022; Received in revised form 14 April 2023; Accepted 15 April 2023
Available online 25 April 2023

theoretically studied for the standard nonlinear Schrödinger equation in Ref. [23]. Exploiting this mechanism for higher-order soliton compression, we achieve record-breaking pulse-compression factors, outperforming recent studies in silicon-nitride waveguides [24]. For instance, the compression of a hyperbolic-secant shaped input pulse of 300 fs, corresponding to a higher-order soliton of order $N = 15$, down to 5.4 fs is achieved on a propagation length of only 6.33 mm. In this respect, diamond allows to consider comparatively high pulse intensities enabling conditions that facilitate high-order soliton propagation effects when pumping in the domain of anomalous dispersion. The fabrication of diamond waveguides with cross-sections that allow to engineer the required dispersion profiles, working at telecom wavelengths and exhibiting the key-feature of a wide domain of anomalous dispersion, is technically feasible [1,25]. In this regard, since silica-based fibers have clear limitations concerning transparency and convenient dispersion profiles (as described in Sect. 2 below), working with diamond seems beneficial, e.g., the ability to engineer unusual dispersion profiles with several zero-dispersion points leads to the observation of new phenomena [26–31].

In Sect. 2 we introduce the numerical model for nonlinear pulse propagation in more detail. Section 3 contains the analysis of the supercontinuum generation process and the pulse self-compression scheme in the considered diamond waveguide. Finally, we discuss our results and conclude in Sect. 4.

2. Methods

For the numerical simulation and analysis of the nonlinear z-propagation dynamics of ultrashort laser pulses we use the generalized nonlinear Schrödinger equation (GNLS) [10,15]

$$\partial_z A = i\sum_{n\geq 2}\frac{\beta_n}{n!}(i\partial_t)^n A + i\gamma\left(1 + i\omega_0^{-1}\partial_t\right) \times \left[A(z,t)\int R(t')|A(z,t-t')|^2\, \mathrm{d}t'\right], \tag{1}$$

for a complex-valued field $A \equiv A(z,t)$ on a periodic time-domain of extend T with boundary condition $A(z,-T/2) = A(z,T/2)$. In Eq. (1), t is a retarded time measured in a reference frame moving with the group velocity at ω_0, where ω_0 is a reference frequency with units rad/ps. The real-valued coefficients β_n specify the dispersion coefficients of order n with units ps^n/m, and γ specifies the nonlinear coefficient with units $\mathrm{W}^{-1}/\mathrm{m}$.

To model dispersive and nonlinear effects in diamond waveguides we use a propagation constant $\beta(\Omega) = \sum_{n\geq 2}(\beta_n/n!)\Omega^n$, where $\Omega = \omega - \omega_0$ defines an angular frequency detuning, characterized by the relative group delay $\beta_1(\Omega) = \partial_\Omega\ \beta(\Omega)$ shown in Fig. 1(a), and group-velocity dispersion $\beta_2(\Omega) = \partial_\Omega^2\ \beta(\Omega)$ shown in Fig. 1(b). This broadband anomalous dispersion profile characterizes a silica embedded diamond waveguide with height $H = 950$ nm and width $W = 875$ nm, extracted from Ref. [1]. This waveguide device was designed for the telecom wavelength range and exhibits a wide domain of anomalous dispersion, bounded by zero dispersion points at $\lambda_{Z1} \approx 843$ nm and $\lambda_{Z2} \approx 2340$ nm, see Fig. 1. We further use $\gamma = 9.6\ \mathrm{W}^{-1}/\mathrm{m}$ [25]. The Raman effect is included via the total response function

$$R(t) = (1 - f_R)\ \delta(t) + f_R\ h_R(t), \tag{2}$$

where the first term defines the instantaneous Kerr response, and where the second term specifies a generic two-parameter Raman response function [32,33]

$$h_R(t) = \frac{\tau_1^2 + \tau_2^2}{\tau_1\tau_2^2}\ e^{-t/\tau_2}\ sin(t/\tau_1)\ \Theta(t), \tag{3}$$

with fractional contribution f_R, with the Heaviside step-function $\Theta(t)$ ensuring causality. To model the Raman effect in diamond waveguides we here use $f_R = 0.20$, $\tau_1 = 4.0$ fs, and $\tau_2 = 5.7$ fs [34]. Using a discrete sequence of angular frequency detunings $\Omega = \omega - \omega_0 \in 2\pi T^{-1}\mathbb{Z}$, the expressions

$$A_\Omega(z) = \frac{1}{T}\int_{-T/2}^{T/2} A(z,t)\ e^{i\Omega t}\ \mathrm{d}t, \tag{4a}$$

$$A(z,t) = \sum_\Omega A_\Omega(z)\ e^{-i\Omega t}, \tag{4b}$$

specify forward [Eq. (4a)], and inverse [Eq. (4b)] Fourier transforms, relating the field envelopes $A(z,t)$ to the spectral envelopes $A_\Omega(z)$. The energy of the field A can be written in the form $E(z) = \hbar\sum_\Omega n_\Omega(z)\ (\omega_0 + \Omega)$, where $\hbar$ is the reduced Planck constant, and where the dimensionless quantity $n_\Omega(z) \equiv T|A_\Omega(z)|^2/[\hbar(\omega_0 + \Omega)]$ specifies the number of photons with energy $\hbar(\omega_0 + \Omega)$. Consequently, the total number of photons is given by

$$C_{\mathrm{Ph}}(z) = \frac{2\pi}{\hbar\Delta\Omega}\sum_\Omega\frac{|A_\Omega(z)|^2}{\omega_0 + \Omega}. \tag{5}$$

Let us note that the GNLS (1) conserves the total number of photons C_{Ph}, but does not conserve the energy E due to the Raman interaction and self-steepening [32]. The numerical simulations in terms of the GNLS reported below are performed using the variable stepsize "conservation quantity error" (CQE) method [35–38], with stepsize selection guided by C_{Ph}. To assess time-frequency interrelations within the field A at a selected propagation distance z, we use the spectrogram [39,40]

$$P_S(t,\Omega) = \frac{1}{2\pi}\left|\int_{-T/2}^{T/2} A(z,t')h(t'-t)e^{-i\Omega t'}\ \mathrm{d}t'\right|^2, \tag{6}$$

wherein $h(x) = exp\left(-x^2/2\sigma^2\right)$ is a Gaussian window function with root-mean-square width σ, allowing to localize A in time.

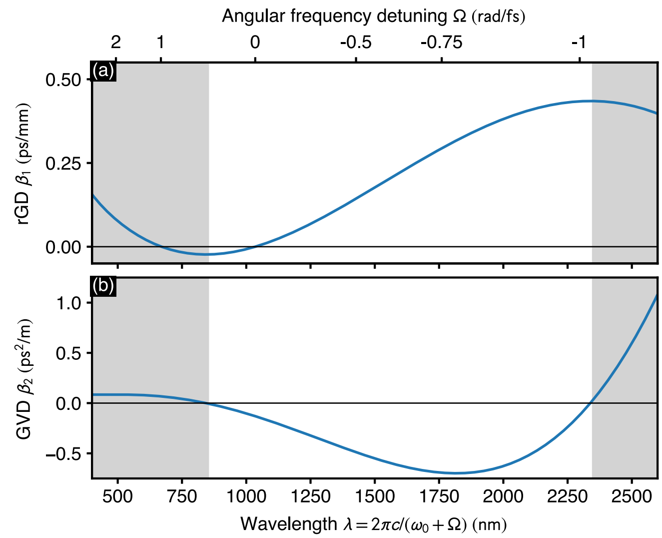

Fig. 1. Characteristics of the propagation constant of the considered diamond waveguide, reproduced following Fig. 5(a) Ref. [1]. (a) Frequency dependence of the relative group delay (rGD). (b) Frequency dependence of the group-velocity dispersion (GVD), with zero-dispersion points are at $\lambda_{Z1} \approx 843$ nm, and $\lambda_{Z2} \approx 2340$ nm. Domains of normal dispersion are shaded gray. Top axis in (a) indicates the detuning Ω, related to the wavelength through $\lambda = 2\pi c/(\omega_0 + \Omega)$ with speed of light c.

3. Results

Supercontinuum generation. Below we compare a supercontinuum generation process in a standard silica-based optical fiber with properties detailed in Ref. [15], to supercontinuum generation in a silica surrounded diamond waveguide exhibiting the dispersion properties detailed in Fig. 1. Results of numerical simulations using initial hyperbolic-secant pulses $A_0(t) = \sqrt{P_0}\ \mathrm{sech}(t/t_0)$ with peak power P_0 and duration t_0 are shown in Fig. 2 (parameters are detailed below). Starting from the spectrally narrow input pulse, the interplay of linear and nonlinear effects inherent to Eq. (1) leads to an enormous spectral broadening. This involves soliton fission, i.e. the successive breakup of the initial pulse into fundamental solitons, see the insets of Fig. 2(a) and Fig. 2(d), for a silica-fiber and a diamond waveguide, respectively. The pulse breakup is accompanied by the generation of dispersive waves in the domain of normal dispersion, extending the spectrum towards the blue side. Due to the Raman effect these solitons experience a self-frequency shift [Fig. 2(b,e)], extending the red side of the spectrum and resulting in a deceleration of the pulses in the time domain [Fig. 2(a, d)]. Under certain conditions, the ejected solitons form strong refractive index barriers that cannot be surpassed by quasi group-velocity matched dispersive waves in the domain of normal dispersion, resulting in reflection processes that further extend the blue side of the spectrum [15,41–43]. Instances of such reflection processes are visible in the spectrograms in Fig. 2(c,f). While both supercontinuum generation processes look very similar regarding the structure of their underlying soliton fission processes, see insets of Fig. 2(a,d), and spectrum, see Fig. 2(b,e), both occur on very different energy scales and propagation distances. Let us note that a fundamental soliton for the silica-based optical fiber with $\beta_2 = -0.011\ \mathrm{ps}^2/\mathrm{m}$, $\gamma = 0.1\ \mathrm{W}^{-1}/\mathrm{m}$, and, say, $t_0 = 0.1\ \mathrm{ps}$, would require a peak power $P_0 \approx 11\ \mathrm{W}$ and yield a soliton period $z_S = (\pi/2)L_D \approx 1.4\ \mathrm{m}$ (dispersion length $L_D = t_0^2/|\beta_2|$). Such a fundamental soliton would have energy $E = 2.2\ \mathrm{pJ}$. In contrast, a diamond waveguide with $\beta_2 = -0.26\ \mathrm{ps}^2/\mathrm{m}$, $\gamma = 9.6\ \mathrm{W}^{-1}/\mathrm{m}$, and $t_0 = 0.1\ \mathrm{ps}$ requires only $P_0 = 2.7\ \mathrm{W}$ and exhibits $z_S \approx 0.006\ \mathrm{m}$. In this case, $E = 0.54\ \mathrm{pJ}$, i.e. the energy required for the fundamental soliton is smaller by about a factor of four. For the supercontinuum generation process shown in Fig. 2, in case of the silica-based optical fiber, the initial pulse had peak power $P_0 = 10\ \mathrm{kW}$ and duration $t_0 = 28.4\ \mathrm{fs}$, injected at $\omega_0 = 2.260\ \mathrm{rad/fs}$ ($\lambda_0 = 835\ \mathrm{nm}$), corresponding to a soliton of order $N \approx 8.7$. In case of the diamond waveguide, $P_0 = 1.66\ \mathrm{kW}$, $t_0 = 20\ \mathrm{fs}$, and $\omega_0 = 1.82\ \mathrm{rad/fs}$ ($\lambda_0 = 1035\ \mathrm{nm}$), corresponding to a soliton of order $N = 7$. Let us point out that while the supercontinuum generation process in the silica fiber develops on a lengthscale of 12 cm, a similar dynamics in case of the diamond waveguide unfolds on merely 6 mm.

Self-compression scheme. The initial stage of the above supercontinuum generation processes, which is characterized by an enormous spectral broadening, allows to identify a pulse compression scheme, which, in the case of the diamond waveguide [Fig. 2(d–f)], proceeds on a propagation scale of less than a millimeter. Subsequently we discuss this initial self-compression of a higher-order soliton, occurring in the time-domain, in more detail. The narrowing of picosecond pulses in a silica-based single-mode optical fiber in a domain of anomalous dispersion was demonstrated experimentally in Ref. [22]. Therein, pulses with initial duration of $t_0 \approx 4\ \mathrm{ps}$ (7 ps FWHM according to Ref. [22]) were compressed to about 1/27 of their initial duration within a fiber of length 320 m. The underlying mechanism builds upon soliton effects: for a negative value of group-velocity dispersion and for high pulse intensities, exceeding that of a fundamental soliton, the resulting chirp

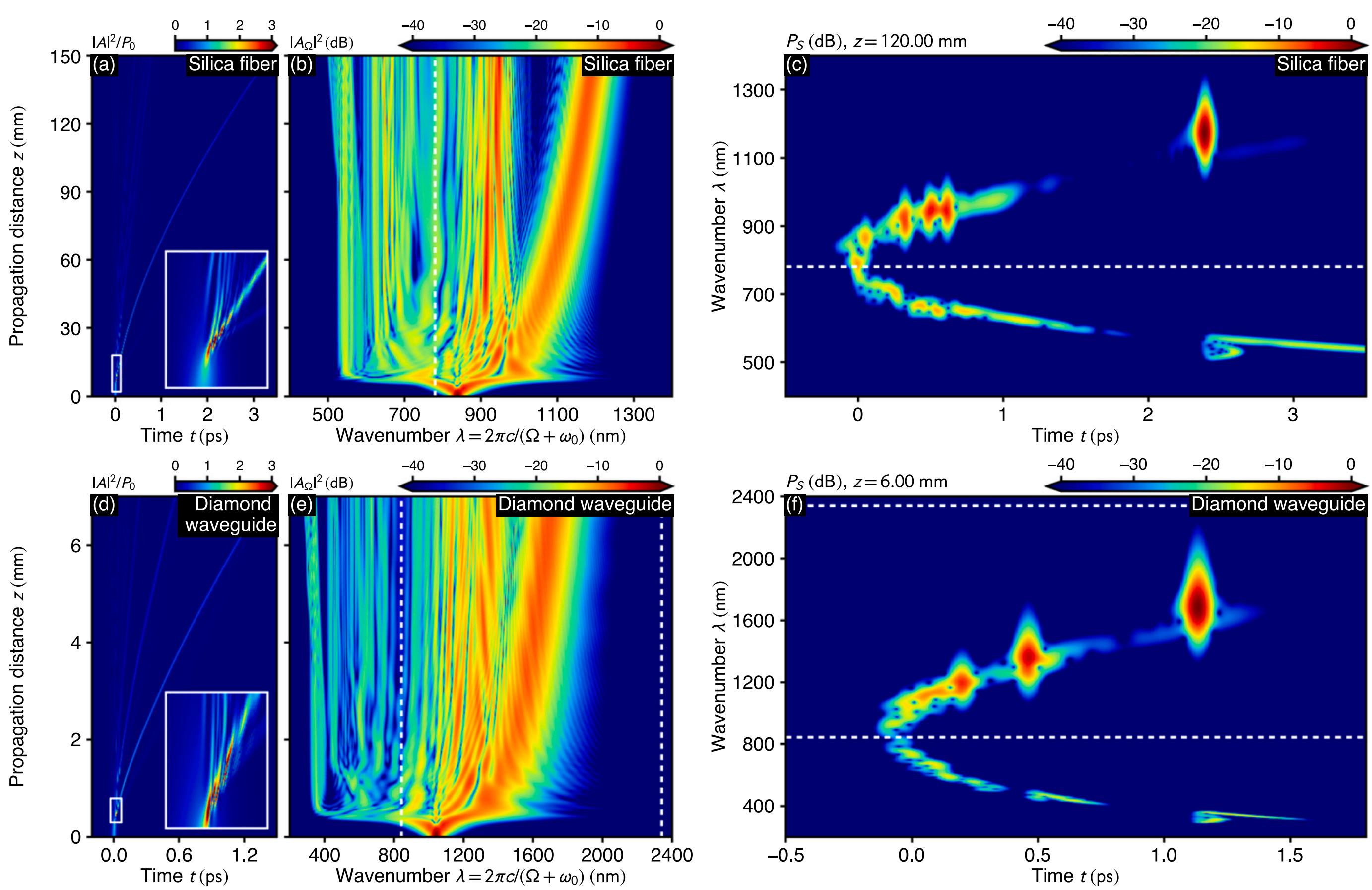

Fig. 2. Supercontinuum generation processes. (a-c) Results for a silica-based optical fiber. (a) Time-domain propagation dynamics. Inset shows zoom-in on the soliton fission process. (b) Spectral-domain propagation dynamics. Vertical dashed line indicates zero-dispersion point at $\lambda_Z \approx 780\ \mathrm{nm}$. (c) Spectrogram at $z = 12\ \mathrm{cm}$ using a rms-width $\sigma = 25\ \mathrm{fs}$ to localize the field. (d–f) Same as (a–c) for a diamond waveguide. Vertical dashed lines in (e) indicate zero-dispersion points at $\lambda_{Z1} \approx 843\ \mathrm{nm}$ and $\lambda_{Z2} \approx 2340\ \mathrm{nm}$.

across the pulse leads to pulse narrowing upon propagation; after the pulse attains maximum compression, soliton fission occurs [see Fig. 2(d)]; the higher the initial intensity, the smaller the propagation distance that is required to reach the point of maximum compression. An analysis of the propagation dynamics of solitons of high order N in terms of the common nonlinear Schrödinger equation (NLS), i.e. Eq. (1) with $f_R = 0$ and nonzero $\beta_2 < 0$ only, yielded results in good qualitative agreement with the experimental findings [22]. A further analysis in terms of numerical simulations for the NLS resulted in the empirical formula $\tau_{\min} = \Delta\tau_0(4.1N)^{-1}$ [23], connecting the half-width $\tau_{\min}$ of the compressed pulse to the initial half-width $\Delta\tau_0$ and accounting for maximum pulse compression by the self-compression (SC) factor

$$F_{\rm SC} = 4.1N, \tag{7}$$

and the optimum self-compression length [23]

$$L_{\rm opt} = \frac{L_D}{N}\left(0.5 + \frac{1.7}{N}\right), \tag{8}$$

where $L_D = t_0^2/|\beta_2|$ is the dispersion length of the initial pulse and $L_{\rm opt}$ specifies the propagation length after which maximum compression is achieved. Considering soliton orders in the range $10 \le N \le 50$, Eq. (8) was found to agree with numerical results for the standard NSE within an accuracy of 2% [23].

Subsequently we transfer the concept of this soliton-effect pulse compression scheme to diamond waveguides with dispersive and nonlinear properties detailed in Sect. 2. Specifically, we consider the operating wavelength $\lambda_0 = 1550$ nm ($\omega_0 = 1.215$ rad/fs), at which $\beta_2(\omega_0) \approx -0.59$ ps^2/m, and hyperbolic secant pulses of duration $t_0 = 0.3$ ps. Figure 3 summarizes the results of our numerical simulations for soliton orders $N = 10$, 15, and, 20. In Fig. 3(a,b) we compare the theoretical predictions of Eqs. (7), (8) with simulations performed in terms of the full GNLS, given by Eq. (1). The good agreement with the above approximate scaling laws does not come as a surprise: during the initial propagation stage, i.e. well before soliton fission sets in, the dynamics is well described by the common NLS. In this regard, an important requirement is that the underlying group-velocity dispersion exhibits a nearly flat anomalous dispersion profile, extending over a wide wavelength range. Problems concerning the compression limit [44], due to an overlap of the spectrally broadened pulse with the domain of normal dispersion, are thus also reduced. For instance, at $N = 15$, we find that the initial pulse compresses down to 5.12 fs, resulting in a self-compression factor $F_{\rm SC} \approx 58$ at the optimal self-compression distance $L_{\rm opt} = 6.33$ mm. Both these values are obtained from pulse propagation simulations in terms of the GNLS (1). Note that for the largest compression factors, the peak intensity might achieve a TW/cm^2 level, in which case higher-order effects such as interband-transitions (multi-photon absorption) start to play an increasing role. A visual account of the achieved compression is given in Fig. 3(c), where the pulse intensity at $L_{\rm opt}$ is compared to its initial trace for the above three choices of N. Similar as in Ref. [22], we observe that for increasing N, an increasingly narrow central peak on top of a broad pedestal emerges. The propagation dynamics for the case $N = 15$ is demonstrated in Fig. 3(d,e): in the propagation range up to $L_{\rm opt}$, the pulse self-compression and increase in peak intensity [Fig. 3(d)], accompanied by spectral broadening [Fig. 3(e)], is clearly evident; immediately beyond $z_{\rm SC}$, soliton fission sets in. Let us emphasize that the considered diamond waveguides support the propagation of ultrashort solitons at rather low pulse intensities. This is a special property enabled by diamond waveguides. Finally, let us note that upon approaching $L_{\rm opt}$, the peak intensity increases at a strongly increasing rate, see Fig. 3(f). This requires an adequate adjustment of the device length or input power to optimally exploit this compression scheme.

In this regard, let us note that under laboratory conditions, further perturbations can render the determination of the optimal self-compression length challenging. For instance, to assess how the presence of loss affects the initial stage of the supercontinuum generation process, we extend the propagation model by including power loss into the linear part of Eq. (1). Similar to Ref. [45], where the impact of loss on the propagation dynamics of solitons in gas-filled hollow-core photonic crystal fibers has been discussed, we assume power loss with 1 dB per (approximate) soliton fission length $L_{\rm fiss} = L_D/N$. As evident from Fig. 3(f), in the presence of loss, the optimal self-compression distance increases, and the associated peak intensity decreases. Specifically, for soliton order $N = 15$ we find an increase from $L_{\rm opt} = 6.33$ mm ($F_{\rm SC} \approx 58$), obtained in absence of loss, to $L_{\rm opt} = 6.59$ mm ($F_{\rm SC} \approx 53$).

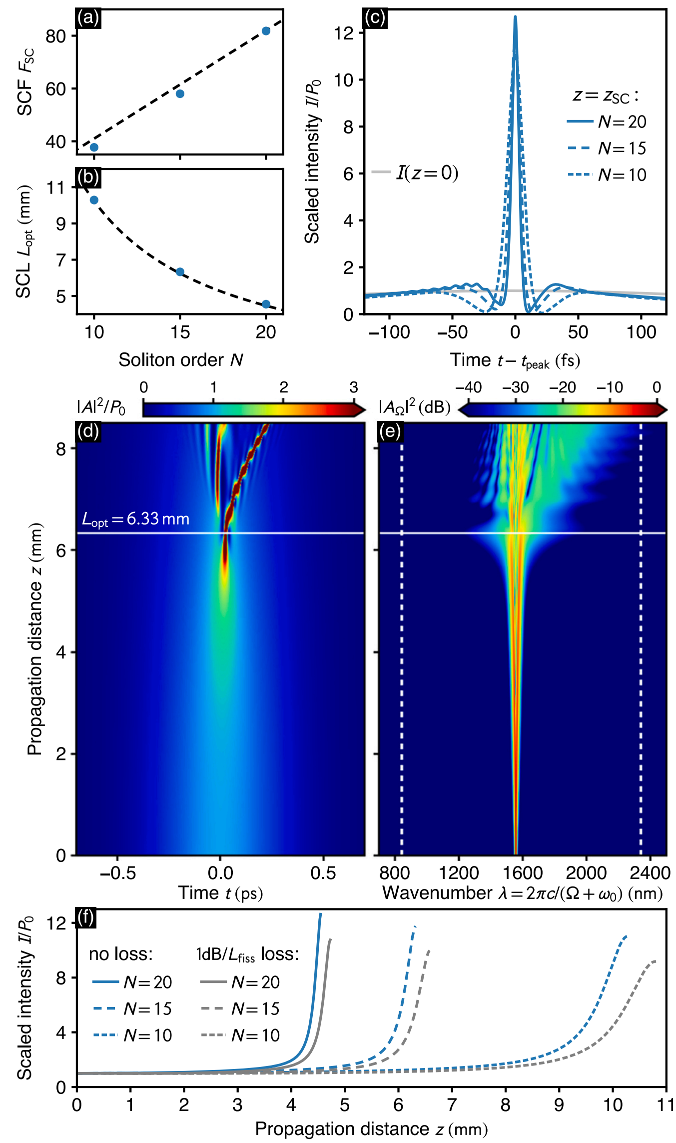

Fig. 3. Pulse compression scheme based on soliton dynamics. (a) Dependence of the soliton self-compression factor (SCF) $F_{\rm SC}$ on the soliton order N. (b) Dependence of the soliton self-compression length (SCL) $L_{\rm opt}$ on N. The scaling laws governing the dashed lines in (a,b) are detailed in the text. Blue dots in (a, b) are the results of numerical simulations in terms of Eq. (1). (c) Intensity profile at $z = L_{\rm opt}$ for soliton orders $N = 10,\ 15,\ 20$, centered on the pulse peak position $t_{\rm peak}$. (d) Propagation dynamics in the time-domain for $N = 15$, and, (e) propagation dynamics in the spectral domain. Horizontal lines in (d,e) indicate the optimal self-compression distance $L_{\rm opt} = 6.33$ mm. Vertical dashed lines in (e) indicate zero-dispersion points. (f) Variation of the pulse intensity upon propagation distance for soliton orders $N = 10,\ 15,\ 20$ with and without loss. When including power loss, we assume 1 dB per soliton fission length $L_{\rm fiss} = L_D/N$.

4. Discussion and conclusions

In summary, we studied the nonlinear propagation dynamics of optical pulses in diamond waveguides in terms of the generalized nonlinear Schrödinger equation. Specifically, we considered a waveguide device, designed for the telecom wavelength range with a wide domain of anomalous dispersion [1]. We demonstrated that the supercontinuum generation process, which for silica-based optical fibers usually occurs on the scale of centimeters or even meters, occurs already on the scale of millimeters. Owing to the strong optical nonlinearity of diamond and the large negative value of the achievable waveguide group-velocity dispersion, this process not only occurs on much shorter propagation scales, it also requires much lower pulse energies. Recognizing that the propagation dynamics prior to soliton-fission is always characterized by pulse narrowing, directly allows to transfer a simple and efficient pulse compression scheme to the diamond platform, promising record-breaking compression factors on chip-size propagation distances.

This compression scheme, which is solely based on soliton effects in a domain of anomalous dispersion, has recently been studied experimentally within SiN waveguides [24]. Therein, pulses with initial duration of $1.2\ \mathrm{ps}$ and soliton order $N \approx 19$ were compressed to about $1/18$ of their initial duration within a low-loss, dispersion engineered waveguide of $40\ \mathrm{cm}$ length. This experimentally achieved compression factor is much below the theoretical prediction $F_{\rm SC} \approx 78$ obtained via Eq. (7). Also, earlier efforts to exploit this self-compression mechanism did not yield compression factors larger than 11 [8,46,47]. Considering the modeling approach in terms of Eq. (1), and neglecting further perturbations, an immediate strategy to increase the compression factor would be to start with an initial pulse in the picosecond range and to use longer propagation distances. In this rather idealized approach, the limitation of this compression scheme is given mainly by the extend of the domain of anomalous dispersion, supporting undisturbed soliton propagation. Let us note that when considering experimental conditions, further perturbations, such as loss, are unavoidable and could render the localization of the interaction length of maximum compression challenging. Thus, under laboratory conditions, other optimization heuristics for the pulse parameters need to be taken into account. For instance, in order to mitigate the effects of power losses, it might be advantageous to strive to keep the self-compression length as short as possible. In such a case, the theoretical estimates provided above constitute a reasonable initial guess for further experimental studies. Besides, we note that power limitations due to ionization, which are not taken into account here, might also play a role, influencing the optimal waveguide length.

While the presented study has a focus on diamond waveguides with a simple geometry, we expect that other waveguide devices fabricated on basis of synthetic diamond, such as angle-etched [48], and fin-shaped structures [49], behave in a qualitatively similar manner. The reported findings are of fundamental interest to nonlinear optics, and provide further insight into the complex propagation dynamics of ultrashort pulses in diamond waveguides.

Declaration of competing interest

The authors declare that they have no known competing financial interests or personal relationships that could have appeared to influence the work reported in this paper.

Data availability

Data will be made available on request.

Acknowledgements

Funding: This work was supported by the Deutsche Forschungsgemeinschaft (DFG) under Germany's Excellence Strategy within the Cluster of Excellence PhoenixD (Photonics, Optics, and Engineering—Innovation Across Disciplines) [EXC 2122, Project No. 390833453], and the European Regional Development Fund for the ‘Hannover Alliance of Research on Diamond (HARD)’ (ZW7-85196513).

References

[1] B.J.M. Hausmann, I. Bulu, V. Venkataraman, P. Deotare, M. Lončar, Diamond nonlinear photonics, Nat. Photonics 8 (2014) 369.
[2] P. Rath, S. Ummethala, C. Nebel, W.H.P. Pernice, Diamond as a material for monolithically integrated optical and optomechanical devices, Phys. Status Solidi A 212 (11) (2015) 2385–2399.
[3] A.L. Gaeta, M. Lipson, T.J. Kippenberg, Photonic-chip-based frequency combs, Nat. Photonics 13 (2019) 158–169.
[4] A. Beveratos, R. Brouri, T. Gacoin, A. Villing, J.-P. Poizat, P. Grangier, Single photon quantum cryptography, Phys. Rev. Lett. 89 (2002), 187901.
[5] B.J.M. Hausmann, I.B. Bulu, P.B. Deotare, M. McCutcheon, V. Venkataraman, M. L. Markham, D.J. Twitchen, M. Lončar, Integrated high-quality factor optical resonators in diamond, Nano Lett. 13 (2013) 1898–1902.
[6] T.J. Kippenberg, R. Holzwarth, S.A. Diddams, Microresonator-based optical frequency combs, Science 332 (2011) 555–559.
[7] W. Ding, C. Benton, A.V. Gorbach, W.J. Wadsworth, J.C. Knight, D.V. Skryabin, M. Gnan, M. Sorrel, R.M.D.L. Rue, Solitons and spectral broadening in long silicon-on-insulator photonic wires, Opt. Express 16 (2008) 3310–3319.
[8] A. Blanco-Redondo, C. Husko, D. Eades, Y. Zhang, J. Li, T.F. Krauss, B.J. Eggleton, Observation of soliton compression in silicon photonic crystals, Nat. Commun. 4 (2010) 3160.
[9] J.K. Ranka, R.S. Windeler, A.J. Stentz, Visible continuum generation in air–silica microstructure optical fibers with anomalous dispersion at 800 nm, Opt. Lett. 25 (2000) 25.
[10] G.P. Agrawal, Nonlinear Fiber Optics, Academic Press, 2019.
[11] F. Mitschke, Fiber Optics: Physics and Technology, Springer, 2016.
[12] D.V. Skryabin, A.V. Gorbach, Colloquium: looking at a soliton through the prism of optical supercontinuum, Rev. Mod. Phys. 82 (2010) 1287–1299.
[13] I. Hartl, X.D. Li, C. Chudoba, R.K. Ghanta, T.H. Ko, J.G. Fujimoto, J.K. Ranka, R. S. Windeler, Ultrahigh-resolution optical coherence tomography using continuum generation in an air–silica microstructure optical fiber, Opt. Lett. 26 (2001) 608–610.
[14] T. Udem, R. Holzwarth, T.W. Hänsch, Optical frequency metrology, Nature 416 (2002) 233–237.
[15] J.M. Dudley, G. Genty, S. Coen, Supercontinuum generation in photonic crystal fiber, Rev. Mod. Phys. 78 (2009) 1135.
[16] F. DeMartini, C.H. Townes, T.K. Gustafson, P.L. Kelley, Self-steepening of light pulses, Phys. Rev. 164 (1967) 312.
[17] J.R. de Oliveira, M.A. de Moura, J.M. Hickmann, A.S.L. Gomes, Self-steepening of optical pulses in dispersive media, J. Opt. Soc. Am. B 9 (1992) 2025.
[18] J.P. Gordon, Theory of the soliton self-frequency shift, Opt. Lett. 11 (1986) 662.
[19] A. Demircan, U. Bandelow, Supercontinuum generation by the modulation instability, Opt. Commun. 244 (2005) 181–185.
[20] A.V. Husakou, J. Herrmann, Supercontinuum generation of higher-order solitons by fission in photonic crystal fibers, Phys. Rev. Lett. 87 (2001), 203901.
[21] A. Demircan, U. Bandelow, Analysis of the interplay between soliton fission and modulation instability in supercontinuum generation, Appl. Phys. B Lasers Opt. 86 (2007) 31.
[22] L.F. Mollenauer, R.H. Stolen, J.P. Gordon, W.J. Tomlinson, Extreme picosecond pulse narrowing by means of soliton effect in single-mode optical fibers, Opt. Lett. 8 (5) (1983) 289–291.
[23] E.M. Dianov, Z.S. Nikonova, A.M. Prokhorov, V.N. Serkin, Optimal compression of multi-soliton pulses in optical fibers, Sov. Tech. Phys. Lett. 12 (1986) 311–313.
[24] R. Oliver, Y. Okawachi, X. Ji, A.R. Johnson, A. Klenner, M. Lipson, A.L. Gaeta, Soliton-effect compression of picosecond pulses on a photonic chip, Opt. Lett. 46 (2021) 4706–4709.
[25] B. Feigel, D. Castelló-Lurbe, H. Thienpont, N. Vermeulen, Opportunities for visible supercontinuum light generation in integrated diamond waveguides, Opt. Lett. 42 (2017) 3804.
[26] V.N. Serkin, V.A. Vysloukh, J.R. Taylor, Soliton spectral tunnelling effect, Electron. Lett. 29 (1993) 12–13.
[27] O. Melchert, S. Willms, S. Bose, A. Yulin, B. Roth, F. Mitschke, U. Morgner, I. Babushkin, A. Demircan, Soliton molecules with two frequencies, Phys. Rev. Lett. 123 (2019), 243905.
[28] K.K.K. Tam, T.J. Alexander, A. Blanco-Redondo, C.M. de Sterke, Generalized dispersion Kerr solitons, Phys. Rev. A 101 (2020), 043822.
[29] E.N. Tsoy, C.M. de Sterke, Theoretical analysis of the self-frequency shift near zero-dispersion points: soliton spectral tunneling, Phys. Rev. A 76 (2007), 043804.
[30] O. Melchert, A. Demircan, Incoherent two-color pulse compounds, Opt. Lett. 46 (2021) 5603.
[31] S. Willms, O. Melchert, S. Bose, A. Yulin, I. Oreshnikov, U. Morgner, I. Babushkin, A. Demircan, Heteronuclear soliton molecules with two frequencies, Phys. Rev. A 105 (2022), 053525.
[32] K.J. Blow, D. Wood, Theoretical description of transient stimulated Raman scattering in optical fibers, IEEE J. Quantum Electron. 25 (1989) 2665.
[33] R.H. Stolen, J.P. Gordon, W.J. Tomlinson, Raman response function of silica-core fibers, J. Opt. Soc. Am. B 6 (1989) 1159.

[34] T.M. Kardás, B. Ratajska-Gadomska, W. Gadomski, A. Lapini, R. Righini, The role of stimulated raman scattering in supercontinuum generation in bulk diamond, Opt. Express 21 (2013) 24201.
[35] A.M. Heidt, Efficient adaptive step size method for the simulation of supercontinuum generation in optical fibers, IEEE J. Lightwave Tech. 27 (2009) 3984.
[36] A.A. Rieznik, A.M. Heidt, P.G. Konig, V.A. Bettachini, D.F. Grosz, Optimum integration procedures for supercontinuum simulation, IEEE Photonics J. 4 (2012) 552–560.
[37] O. Melchert, A. Demircan, py-fmas: a python package for ultrashort optical pulse propagation in terms of forward models for the analytic signal, Comput. Phys. Commun. 273 (2022), 108257.
[38] O. Melchert, A. Demircan, GNLStools.py: a generalized nonlinear Schrödinger python module implementing different models of input pulse quantum noise, SoftwareX 20 (2022), 101232.
[39] O. Melchert, B. Roth, U. Morgner, A. Demircan, OptFROG — analytic signal spectrograms with optimized time–frequency resolution, SoftwareX 10 (2019), 100275.
[40] L. Cohen, Time-frequency distributions – a review, Proc. IEEE 77 (1989) 941–981.
[41] R. Driben, F. Mitschke, N. Zhavoronkov, Cascaded interactions between Raman induced solitons and dispersive waves in photonic crystal fibers at the advanced stage of supercontinuum generation, Opt. Express 18 (25) (2010) 25993–25998.
[42] A. Demircan, S. Amiranashvili, C. Brée, G. Steinmeyer, Compressible octave spanning supercontinuum generation by two-pulse collisions, Phys. Rev. Lett. 110 (2013), 233901.
[43] A. Demircan, S. Amiranashvili, C. Brée, U. Morgner, G. Steinmeyer, Adjustable pulse compression scheme for generation of few-cycle pulses in the midinfrared, Opt. Lett. 39 (2014) 2735.
[44] A. Demircan, M. Kroh, U. Bandelow, B. Hüttl, H.-G. Weber, Compression limit by third-order dispersion in the normal dispersion regime, IEEE Photon. Technol. Lett. 18 (2006) 2353–2355.
[45] J.C. Travers, W. Chang, J. Nold, N.Y. Joly, P.S.J. Russell, Ultrafast nonlinear optics in gas-filled hollow-core photonic crystal fibers [Invited], J. Opt. Soc. Am. B 28 (2011) A11–A26.
[46] P. Colman, C. Husko, S. Combrié, I. Sagnes, C.W. Wong, A. De Rossi, Temporal solitons and pulse compression in photonic crystal waveguides, Nat. Photonics 4 (2010) 862–868.
[47] J.W. Choi, B.-U. Sohn, G.F.R. Chen, D.K.T. Ng, D.T.H. Tan, Soliton-effect optical pulse compression in CMOS-compatible ultra-silicon-rich nitride waveguides, APL Photonics 11 (2019), 110804.
[48] A. Shams-Ansari, P. Latawiec, Y. Okawachi, V. Venkataraman, M. Yu, B. Desiatov, H. Atikian, G.L. Harris, N. Picqué, A.L. Gaeta, M. Lončar, Supercontinuum generation in angle-etched diamond waveguides, Opt. Lett. 44 (2019) 4056–4059.
[49] R.R. Grote, L.C. Bassett, Single-mode optical waveguides on native high-refractive-index substrates, APL Photonics 1 (2016), 071302.